Self-consistent separable random-phase approximation for Skyrme forces: Giant resonances in axial nuclei

V. O. Nesterenko,[1] W. Kleinig,[1,2] J. Kvasil,[3] P. Vesely,[3] P.-G. Reinhard,[4] and D. S. Dolci[1]
[1]*Laboratory of Theoretical Physics, Joint Institute for Nuclear Research, Dubna, Moscow region, 141980, Russia**
[2]*Technische Universität Dresden, Institut für Analysis, D-01062 Dresden, Germany*
[3]*Institute of Particle and Nuclear Physics, Charles University, CZ-18000 Praha 8, Czech Republic,*
[4]*Institut für Theoretische Physik II, Universität Erlangen, D-91058 Erlangen, Germany*
(Received 7 September 2006; published 8 December 2006)

We formulate the self-consistent separable random phase approximation (SRPA) method and specify it for Skyrme forces with pairing for the case of axially symmetric deformed nuclei. The factorization of the residual interaction allows diagonalization of high-ranking RPA matrices to be avoided, which dramatically reduces the computational expense. This advantage is crucial for the systems with a huge configuration space, first of all for deformed nuclei. SRPA self-consistently takes into account the contributions of both time-even and time-odd Skyrme terms as well as of the Coulomb force and pairing. The method is implemented to describe isovector E1 and isoscalar E2 giant resonances in a representative set of deformed nuclei: ^{154}Sm, ^{238}U, and ^{254}No. Four different Skyrme parameterizations (SkT6, SkM*, SLy6, and SkI3) are employed to explore the dependence of the strength distributions on some basic characteristics of the Skyrme functional and nuclear matter. In particular, we discuss the role of isoscalar and isovector effective masses and their relation to time-odd contributions. The high sensitivity of the right flank of E1 resonance to different Skyrme forces and the related artificial structure effects are analyzed.

DOI: 10.1103/PhysRevC.74.064306 PACS number(s): 21.30.Fe, 21.60.Ev, 21.60.Jz, 24.30.Cz

I. INTRODUCTION

Self-consistent mean-field models with effective energy-density functionals (Skyrme-Hartree-Fock, Gogny, relativistic) are established as reliable tools for the description of nuclear structure and dynamics; for a comprehensive review see Ref. [1]. In particular, there is a rising implementation of these models to dynamical features of nuclei (see, e.g., Refs. [2–6]), which is caused, to a large extent, by exploiting the spectra and reaction rates of exotic nuclei in astrophysics [7,8]. However, applications of self-consistent models to nuclear dynamics are still limited even in the linear regime which is usually treated within the random phase approximation (RPA). The calculations are plagued by dealing with high-ranking RPA matrices. This is especially difficult for deformed systems where lack of symmetry requires a huge one-particle-one-hole ($1ph$) configuration space.

The RPA problem becomes much simpler if the residual two-body interaction is factorized (i.e., reduced to a separable form):

$$\sum_{p_1h_1ph} \langle p_1h_1|V_{\rm res}|ph\rangle\ a^+_{p_1}a^+_{h_1}a_pa_h \to \sum_{k,k'=1}^{K} \kappa_{k,k'}\hat{X}_k\hat{X}_{k'}, \quad (1)$$

where $\hat{X}_k = \sum_{ph}\langle p|\hat{X}_k|h\rangle a^+_pa_h$ is a hermitian $1ph$ operator and $\kappa_{kk'}$ is a matrix of strength constants. The factorization allows the reduction of a high-ranking RPA matrix to a much smaller one with a rank of 4K (where the coefficient 4 is caused by the isospin and time-parity factors, see discussion in the next section). The separable expansion can be formulated in a fully self-consistent manner and provide a high accuracy with a small number ($K \sim$ 2–6) of the separable terms.

Several self-consistent schemes for separable expansions have been proposed during the last decades [9–16]. However, these schemes are not sufficiently general. Some of them are limited to analytical or simple numerical estimates [9–12]; the others are not fully self-consistent [14]. Between them the approach [15,16] for Skyrme forces is quite promising. However, it still deals with RPA matrices of rather high rank ($\sim$400).

Recently, we have developed a general self-consistent separable RPA (SRPA) approach applicable to arbitrary density- and current-dependent functionals [17–23]. The method was implemented to the Skyrme functional [1,24–26] for both spherical [19–22] and deformed [23] nuclei. In SRPA, the one-body operators $\hat{X}_k$ and associated strengths $\kappa_{k,k'}$ are unambiguously derived from the given energy-density functional. There remain no further adjustable parameters. The success of the expansion depends on an appropriate choice of the basic operators $\hat{X}_k$. Experience with spherical SRPA gives guidelines for an efficient choice such that a few separable terms suffice to reproduce accurately the exact RPA spectra [19–21]. The success becomes possible because of the following factors: (i) an efficient self-consistent procedure [9,11] based on sound physical arguments; (ii) proper inclusion of all parts of the residual interaction, time-even as well as time-odd couplings; (iii) incorporation of the symmetries (translation, particle number, etc.) leading to a correct description of the related zero-energy modes; and (iv) building the separable operators in such a way that they have maxima at different slices of the nucleus and thus cover both surface and interior

*Electronic address: nester@theor.jinr.ru

dynamics. Furthermore, we note that SRPA is very general and can be applied to a wide variety of finite Fermion systems. For example, SRPA was derived for the Kohn-Sham functional [27,28] and widely used for description of linear dynamics of valence electrons in spherical and deformed atomic clusters [17,18,29–32].

The enormous reduction of computational expense by SRPA is particularly advantageous for deformed systems where 1*ph* configuration space grows huge. SRPA becomes here a promising tool for large scale studies. It is the aim of this article to present a first implementation of SRPA for axially deformed nuclei with pairing. Like the full RPA, SRPA follows two strategies to compute the dynamical response. It can be calculated via determination of RPA eigenvalues and eigenstates or by a direct computation of the multipole strength functions related to experimental cross sections. We discuss both ways.

As a first test, we apply the method to the description of isovector E1 and isoscalar E2 giant resonances (GR) in the deformed nuclei ^{154}Sm, ^{238}U, and ^{254}No. These nuclei cover a broad size range from rare-earth to superheavy elements. Four different Skyrme forces (SkT6 [33], SkM* [34], SLy6 [35], and SkI3 [36]) are used to explore the dependence of the results on the actual parametrization. For our aims it is important that these forces represent different values of some relevant nuclear matter characteristics (isoscalar and isovector effective masses and asymmetry energy). We discuss the dependence of the collective strength on these characteristics, scrutinize the impact of time-odd coupling terms in the Skyrme residual interaction, and demonstrate the important role of the Landau fragmentation.

The article is organized as follows. The general SRPA formalism is presented in Sec. II and specified for Skyrme forces in Sec. III. In Sec. IV we discuss the choice of input operators. Results of the calculations are analyzed in Sec. V. The summary is done in Sec. VI. Some important details of the method are given in Appendices A–C. For more details, see documentation in Ref. [23].

II. BASIC SRPA EQUATIONS

A. The separable expansion

In the most general form, the factorization of the residual interaction (1) reads

$$\hat{V}_{\rm res} \to \hat{V}_{\rm res}^{\rm sep} = -\frac{1}{2}\sum_{ss'}\sum_{k,k'=1}^{K}\{\kappa_{sk,s'k'}\hat{X}_{sk}\hat{X}_{s'k'} + \eta_{sk,s'k'}\hat{Y}_{sk}\hat{Y}_{s'k'}\}, \tag{2}$$

where the indices s and s' label neutrons and protons, $\hat{X}_{sk}$ are time-even hermitian one-body operators and $\hat{Y}_{sk}$ are their time-odd counterparts, and $\kappa_{sk,s'k'}$ and $\eta_{sk,s'k'}$ are the strength matrices. Time reversal properties of the operators are

$$\begin{aligned} T\hat{X}_{sk}T^{-1} &= \gamma_T^X\hat{X}_{sk}, \quad \gamma_T^X = +1, \\ T\hat{Y}_{sk}T^{-1} &= \gamma_T^Y\hat{Y}_{sk}, \quad \gamma_T^Y = -1, \end{aligned} \tag{3}$$

where T is the operator of time reversal. The expansion (2) needs to take care of both classes of operators because the relevant Skyrme functionals involve both time-even and time-odd couplings; see Ref. [1] and Appendix A. Though time-odd variables do not contribute to the *static* mean field Hamiltonian of spin-saturated systems, they can play a role in time-dependent perturbations and nuclear dynamics. Altogether, the presence of time-even and time-odd couplings in the functional naturally leads to the formulation of the separable model in terms of hermitian operators with a given time-parity. These operators have the useful property

$$\langle[\hat{A},\hat{B}]\rangle \sim \left(1-\gamma_T^A\gamma_T^B\right), \tag{4}$$

which means that the average value of the commutator at the ground state $|\,\rangle$ is not zero only for operators of the opposite T parities ($\gamma_T^A = -\gamma_T^B$). This property is widely used in the following.

B. Linearized time-dependent mean field

RPA is the limit of small-amplitude harmonic vibrations around the ground state. The dynamics is formulated in general by a time-dependent variation on the basis of a given energy functional $E(J_s^\alpha(\vec{r},t))$,

$$\langle\Psi(t)|\hat{H}|\Psi(t)\rangle \longrightarrow E\left(J_s^\alpha(\vec{r},t)\right) = \int \mathcal{H}(\vec{r},t)d\vec{r}. \tag{5}$$

We deal with a set of densities $J_s^\beta(\vec{r})$, where β denotes the type of density (spatial density, kinetic density, current, spin density, spin-orbit density, etc.) and s labels protons and neutrons. For reasons of compact notation, we combine the density type β with the space point $\vec{r}$ into one index α such that

$$\alpha \equiv (\beta,\vec{r}), \quad \sum_\alpha \ldots = \sum_\beta \int d\vec{r}\ldots \tag{6}$$

The densities are related to the corresponding one-body operators $\hat{J}_s^\alpha$ (see the list in Appendix A) as

$$J_s^\alpha(t) = \langle\Psi(t)|\hat{J}_s^\alpha|\Psi(t)\rangle = \sum_{h\in s} v_h^2\varphi_h^*(t)\hat{J}_s^\alpha\varphi_h(t). \tag{7}$$

Further, the state $|\Psi(t)\rangle$ is the underlying Bardeen-Cooper-Schrieffer (BCS) mean-field state composed from the single-particle states $\varphi_h(\vec{r},t)$ and the corresponding pairing occupation amplitudes v_h. The time evolution is determined by variation of the action $\langle\Psi(t)|i\partial_t|\Psi(t)\rangle - \int d\vec{r}\mathcal{H}(\vec{r},t)$. Till now we keep the occupation amplitudes v_h fixed at their ground state values and consider the variation of the single-particle states. This yields the time-dependent mean-field equations as

$$i\frac{d}{dt}\varphi_h = \hat{h}\varphi_h, \tag{8}$$

with the mean field Hamiltonain $\hat{h}$ being a functional of the local and instantaneous densities $J_s^\alpha(\vec{r},t)$. The freezing of the occupation amplitudes v_h somewhat inhibits application of SRPA for vibrational modes with a strong pairing impact (e.g., for low-lying modes in neutron-rich light deformed nuclei) [37]. However, in the present study we are interested in giant resonances where pairing dynamics plays a minor role.

In the linear regime of small amplitude oscillations, the time-dependent state consists of the static ground state $|\,\rangle$ and a small time-dependent perturbation

$$|\Psi(t)\rangle = |\,\rangle + |\delta\Psi(t)\rangle, \tag{9}$$

where both $|\Psi(t)\rangle$ and $|\,\rangle$ are BCS states. Hence, all dynamical quantities can be decomposed as a sum of the stationary ground state and small time-dependent parts:

$$J_s^\alpha(\vec{r},t) = \tilde{J}_s^\alpha(\vec{r}) + \delta J_s^\alpha(\vec{r},t), \tag{10a}$$

$$\delta J_s^\alpha(\vec{r},t) = \langle\Psi(t)|\hat{J}_s^\alpha|\Psi(t)\rangle - \langle\hat{J}_s^\alpha\rangle. \tag{10b}$$

Inserting Eq. (10) into Eq. (5) and keeping the terms up to the first order in $\delta J_s^\alpha(\vec{r},t)$, one obtains the single-particle Hamiltonian

$$\hat{h}(t) = \hat{h}_0 + \hat{h}_{\rm res}(t), \tag{11}$$

with the static mean-field part

$$\hat{h}_0 = \sum_{\alpha s} \frac{\delta E}{\delta J_s^\alpha}\hat{J}_s^\alpha \tag{12}$$

and the time-dependent response

$$\hat{h}_{\rm res}(t) = \sum_{\alpha' s'} \frac{\delta\hat{h}}{\delta J_{s'}^{\alpha'}}\,\delta J_{s'}^{\alpha'}(t) \tag{13}$$

$$= \sum_{\alpha s\alpha' s'} \frac{\delta^2 E}{\delta J_s^\alpha \delta J_{s'}^{\alpha'}}\Big|_{J=\bar{J}}\hat{J}_s^\alpha\,\delta J_{s'}^{\alpha'}(t) \tag{14}$$

related to the oscillations of the system. Note that the second functional derivative is to be taken at the ground state density as indicated by the index $J = \bar{J}$. This holds for all second functional derivatives and so we skip this explicit index in the following. For the brevity of notation, we also skip the explicit dependencies on space coordinates and come back to these details in Sec. III where the residual interaction for the Skyrme functional is worked out.

The linearized equation of motion reads

$$\left(i\frac{d}{dt} - \hat{h}_0\right)|\delta\Psi\rangle = \hat{h}_{\rm res}|\,\rangle. \tag{15}$$

Further steps require a more specific view of $|\delta\Psi\rangle$. This is done in the next subsections from different points of view, macroscopic and microscopic.

C. Macroscopic part of SRPA

1. Scaling perturbed wave function

It is convenient to obtain the perturbed mean-field state $|\Psi(t)\rangle$ by the scaling transformation [11]

$$|\Psi(t)\rangle_s = \prod_{k=1}^{K}\exp[-iq_{sk}(t)\hat{P}_{sk}]\exp[-ip_{sk}(t)\hat{Q}_{sk}]|\rangle_s, \tag{16}$$

where both $|\Psi(t)\rangle_s$ and $|\,\rangle_s$ are the Slater determinants and $\hat{Q}_{sk}(\vec{r})$ and $\hat{P}_{sk}(\vec{r})$ are generalized coordinate (time-even) and momentum (time-odd) hermitian one-body operators. These operators fulfill the properties

$$\hat{Q}_{sk} = \hat{Q}_{sk}^\dagger, \quad \gamma_T^Q = 1, \tag{17a}$$

$$\hat{P}_{sk} = i[\hat{H},\hat{Q}_{sk}] = \hat{P}_{sk}^\dagger, \quad \gamma_T^P = -1 \tag{17b}$$

where $\hat{H} = \hat{h}_0 + \hat{V}_{\rm res}$ stands for the full Hamiltonian embracing both the one-body mean-field Hamiltonian and the two-body residual interaction. The commutator in Eq. (17b) is assumed to be mapped into the one-body domain [see, e.g., the mapping into $\hat{h}_{\rm res}$ in Eq. (19)]. If the functional includes only time-even densities, then $\hat{V}_{\rm res}$ does not contribute to the commutator and so $\hat{H}$ can be safely replaced by $\hat{h}_0$.

2. Separable operators and strength constants

The operators (17) generate time-even and time-odd real collective deformations $q_{sk}(t)$ and $p_{sk}(t)$. Using Eq. (16) and assuming only small deformations, the transition densities (10b) read

$$\delta J_s^\alpha(t) = i\sum_k\{q_{sk}(t)\langle[\hat{P}_{sk},\hat{J}_s^\alpha]\rangle + p_{sk}(t)\langle[\hat{Q}_{sk},\hat{J}_s^\alpha]\rangle\}, \tag{18}$$

where, following Eq. (4), time-even densities contribute only to responses $\langle|[\hat{P}_{sk},\hat{J}_s^\alpha]|\rangle$ while time-odd ones contribute only to $\langle|[\hat{Q}_{sk},\hat{J}_s^\alpha]|\rangle$. Then the response Hamiltonian (13) recasts as

$$\hat{h}_{\rm res}(t) = \sum_{sk}\{q_{sk}(t)\hat{X}_{sk} + p_{sk}(t)\hat{Y}_{sk}\}, \tag{19}$$

where the time dependence is concentrated in the amplitudes $q_{sk}(t)$ and $p_{sk}(t)$ while all time-independent terms are collected in the hermitian one-body operators

$$\hat{X}_{sk} = \sum_{s'}\hat{X}_{sk}^{s'} = i\sum_{\alpha'\alpha s'}\frac{\delta^2 E}{\delta J_{s'}^{\alpha'}\delta J_s^\alpha}\langle[\hat{P}_{sk},\hat{J}_s^\alpha]\rangle\hat{J}_{s'}^{\alpha'}, \tag{20a}$$

$$\hat{Y}_{sk} = \sum_{s'}\hat{Y}_{sk}^{s'} = i\sum_{\alpha'\alpha s'}\frac{\delta^2 E}{\delta J_{s'}^{\alpha'}\delta J_s^\alpha}\langle[\hat{Q}_{sk},\hat{J}_s^\alpha]\rangle\hat{J}_{s'}^{\alpha'}, \tag{20b}$$

with the properties

$$\hat{X} = \hat{X}^\dagger, \quad \gamma_T^X = +1, \quad \hat{X}^* = \hat{X}, \tag{21a}$$

$$\hat{Y} = \hat{Y}^\dagger, \quad \gamma_T^Y = -1, \quad \hat{Y}^* = -\hat{Y}. \tag{21b}$$

Obviously, $\hat{X}_{sk}$ and $\hat{Y}_{sk}$ are the reasonable candidates for the time-even and time-odd operators in the separable expansion (2). The operator $\hat{X}_{sk}$ involves contributions only from the time-even densities while the operator $\hat{Y}_{sk}$ only from the time-odd ones. The upper index s' in the operators (20) determines the isospin (proton or neutron) subspace where these operators act. This is the domain of the involved density operators $\hat{J}_{s'}^{\alpha'}$.

To complete the construction of the separable expansion (2), we should determine the matrices of the strength constants $\kappa_{sk,s'k'}$ and $\eta_{sk,s'k'}$. This can be done through

variations of the basic operators

$$\delta X_{sk}(t) = \langle\Psi(t)|\hat{X}_{sk}|\Psi(t)\rangle - \langle\hat{X}_{sk}\rangle = i\sum_{s'k'} q_{s'k'}(t)\langle\big[\hat{P}_{s'k'}, \hat{X}^{s'}_{sk}\big]\rangle = -\sum_{s'k'} q_{s'k'}(t)\kappa^{-1}_{s'k',sk}, \tag{22a}$$

$$\delta Y_{sk}(t) = \langle\Psi(t)|\hat{Y}_{sk}|\Psi(t)\rangle - \langle\hat{Y}_{sk}\rangle = i\sum_{s'k'} p_{s'k'}(t)\langle\big[\hat{Q}_{s'k'}, \hat{Y}^{s'}_{sk}\big]\rangle = -\sum_{s'k'} p_{s'k'}(t)\eta^{-1}_{s'k',sk}\ , \tag{22b}$$

where

$$\kappa^{-1}_{s'k',sk} = \kappa^{-1}_{sk,s'k'} = -i\langle\big[\hat{P}_{s'k'}, \hat{X}^{s'}_{sk}\big]\rangle = \sum_{\alpha\alpha'}\frac{\delta^2 E}{\delta J^{\alpha'}_{s'}\delta J^{\alpha}_{s}}\langle\big[\hat{P}_{sk}, \hat{J}^{\alpha}_{s}\big]\rangle\langle\big[\hat{P}_{s'k'}, \hat{J}^{\alpha'}_{s'}\big]\rangle, \tag{23a}$$

$$\eta^{-1}_{s'k',sk} = \eta^{-1}_{sk,s'k'} = -i\langle\big[\hat{Q}_{s'k'}, \hat{Y}^{s'}_{sk}\big]\rangle = \sum_{\alpha\alpha'}\frac{\delta^2 E}{\delta J^{\alpha'}_{s'}\delta J^{\alpha}_{s}}\langle\big[\hat{Q}_{sk}, \hat{J}^{\alpha}_{s}\big]\rangle\langle\big[\hat{Q}_{s'k'}, \hat{J}^{\alpha'}_{s'}\big]\rangle. \tag{23b}$$

Equations (23) represent the elements of the symmetric matrices that are inverse to the matrices of the strength constants in Eq. (2). Indeed, Eqs. (22) can be recast to

$$-\sum_{sk}\kappa_{s'k',sk}\delta X_{sk}(t) = q_{s'k'}(t), \tag{24a}$$

$$-\sum_{sk}\eta_{s'k',sk}\delta Y_{sk}(t) = p_{s'k'}(t). \tag{24b}$$

From that we read off the response Hamiltonian (19) as

$$\hat{h}_{\rm res}(t) = -\sum_{s'k'}\sum_{sk}\{\kappa_{s'k',sk}\delta\hat{X}_{sk}(t)\hat{X}_{s'k'} + \eta_{s'k',sk}\delta\hat{Y}_{sk}(t)\hat{Y}_{s'k'}\}, \tag{25}$$

which leads within the collective space of the generators $\{\hat{P}_{sk}\ ,\ \hat{Q}_{sk}\}$ to the same eigenvalue problem as the separable Hamiltonian

$$\hat{H} = \hat{h}_0 + \hat{V}^{\rm sep}_{\rm res}, \tag{26}$$

with $\hat{V}^{\rm sep}_{\rm res}$ given in Eq. (2) (see Refs. [9,19]).

In principle, we already have at our disposal the macroscopic SRPA formalism for a linear regime of the collective motion in terms of real harmonic variables

$$q_{sk}(t) = \bar{q}_{sk}\cos(\omega t) = \frac{1}{2}\bar{q}_{sk}(e^{i\omega t} + e^{-i\omega t}), \tag{27a}$$

$$p_{sk}(t) = \bar{p}_{sk}\sin(\omega t) = \frac{1}{2i}\bar{p}_{sk}(e^{i\omega t} - e^{-i\omega t}). \tag{27b}$$

Indeed, Eqs. (20) and (23) deliver the one-body operators and strength matrices for the separable expansion of the two-body interaction. By substituting the response Hamiltonian (25) and the perturbed wave function (16) into the time-dependent HF Eq. (15), one gets the eigenvalue problem. The number K of the collective variables (and thus of the separable terms) is dictated by the accuracy we need in the description of collective modes. For $K = 1$, the method in fact is reduced to the sum rule approach with one collective mode [38]. For $K > 1$, we have a system of K coupled oscillators and the method becomes similar to so-called local RPA [38,39] suitable for description of the branching and gross-structure of collective modes.

D. Microscopic part of SRPA

The macroscopic SRPA as outlined in Sec. II C serves here as a convenient tool to derive the optimal separable expansion. But it cannot describe the Landau fragmentation of the collective strength. For this aim, we should build the microscopic part of the model. In what follows, we consider the eigenvalue problem and the direct computation of the strength function.

The perturbation $|\delta\Psi\rangle$ belongs to the tangential space of the variations of a mean-field state. For the pure Slater states, they are all conceivable one-particle-one-hole ($1ph$) excitations:

$$\hat{A}^{\dagger}_{ph} = a^{\dagger}_{p}a_{h}, \quad \hat{A}_{ph} = a^{\dagger}_{h}a_{p}. \tag{28}$$

In the BCS case, the elementary modes are reduced to the two-quasiparticle ($2qp$) excitations $\hat{A}^{\dagger}_{ph} \longrightarrow \hat{A}^{\dagger}_{ij} = \hat{\alpha}^{\dagger}_{i}\hat{\alpha}^{\dagger}_{\bar{j}}$, where $\hat{\alpha}^{\dagger}_{j}$ generates the BCS quasiparticle state j and $\bar{j}$ is its time reversal. Just this case is employed in our actual calculations. Both $1ph$ and $2qp$ excitations have much in common and result in the same microscopic SRPA equations (with the exception of pairing peculiarities outlined in Appendix C). So, in what follows, we do not distinguish these two cases. In particular, we use for both excitations one and the same notation, ph.

1. Eigenvalue problem

To formulate the eigenvalue problem, we exploit the standard RPA technique for the separable Hamiltonian (26) where the separable operators and strength constants are delivered by the macroscopic SRPA; see Eqs. (20) and (23). Following [9], the collective motion is represented in terms of

$$|\Psi(t)\rangle_{\nu} = \exp\big(\hat{C}^{\dagger}_{\nu}e^{-i\omega_{\nu}t} - \hat{C}_{\nu}e^{+i\omega_{\nu}t}\big)|\ \rangle, \tag{29a}$$

$$\hat{C}^{\dagger}_{\nu} = \sum_{s}\sum_{ph\in s}\big(c^{\nu-}_{ph}\hat{A}^{\dagger}_{ph} - c^{\nu+}_{ph}\hat{A}_{ph}\big)\ , \tag{29b}$$

where $\hat{C}^{\dagger}_{\nu}$ creates the one-phonon eigenmode ν; the operators $\hat{A}^{\dagger}_{ph}$ and $\hat{A}_{ph}$ are defined in Eq. (28); the perturbed $|\Psi(t)\rangle_{\nu}$ and ground $|\ \rangle$ states have the form of Slater determinants. We employ here the Thouless theorem [40], which establishes connection between two arbitrary Slater determinants. The wave function (29) is a microscopic counterpart of macroscopic scaling ansatz (16). But here we aim for a fully *microscopic* description of excitations covering all the $1ph$ space, whereas in the previous sections we consider *macroscopic* flow as a benchmark for forming the separable interaction.

The time-dependent response Hamiltonian $\hat{h}_{\rm res}(t)$ for the mode $\hat{C}^\dagger_\nu e^{-i\omega_\nu t}$ and the separable interaction (2) reads

$$\hat{h}^\nu_{\rm res} = \sum_{sk} \hat{X}_{sk} \underbrace{\sum_{s'k'} \kappa_{sk,s'k'} \langle [\hat{X}_{s'k'}, \hat{C}^\dagger_\nu] \rangle}_{\bar{q}^\nu_{sk}} + \sum_{sk} \hat{Y}_{sk} \underbrace{\sum_{s'k'} \eta_{sk,s'k'} \langle [\hat{Y}_{s'k'}, \hat{C}^\dagger_\nu] \rangle}_{-i\bar{p}^\nu_{sk}}, \quad (30)$$

where

$$\bar{q}^\nu_{sk} = \sum_{s'k'} \kappa_{sk,s'k'} \cdot \sum_{s''} \sum_{ph\in s''} \langle ph | \hat{X}^{s'_{}}_{s'k'} \rangle (c^{\nu-}_{ph} + c^{\nu+}_{ph}), \quad (31a)$$

$$\bar{p}^\nu_{sk} = i \sum_{s'k'} \eta_{sk,s'k'} \cdot \sum_{s''} \sum_{ph\in s''} \langle ph | \hat{Y}^{s''}_{s'k'} \rangle (c^{\nu-}_{ph} - c^{\nu+}_{ph}). \quad (31b)$$

Note that here the values $\bar{q}^\nu_{sk}$ and $\bar{p}^\nu_{sk}$ are new objects generated by the eigenmode $\hat{C}^\dagger_\nu$. They serve for notation of $\hat{h}_{\rm res}$ and have no relation to the collective generators $\bar{q}_{sk}$, $\bar{p}_{sk}$ used in Sec. II C. Substituting the ansatz (29) into the linearized time-dependent HF equation (15) and employing the form (30) for the response field yields the expression for $1ph$ expansion coefficients

$$c^{\nu\pm}_{ph\in s} = -\sum_{s'k'} \frac{\bar{q}^\nu_{s'k'} \langle ph | \hat{X}^s_{s'k'} \rangle \mp i\, \bar{p}^\nu_{s'k'} \langle ph | \hat{Y}^s_{s'k'} \rangle}{2(\varepsilon_{ph} \pm \omega_\nu)}, \quad (32)$$

where ε_{ph} is the unperturbed energy of $1ph$ pair. In the derivation above we use the operator properties (21). Then the matrix elements $\langle ph|\hat{X}^{s''}_{s'k'}\rangle$ and $\langle ph|\hat{Y}^{s''}_{s'k'}\rangle$ are real and image, respectively, while all the unknowns $c^{\nu\pm}_{ph}$, $\bar{q}^\nu_{sk}$ and $\bar{p}^\nu_{sk}$ are real.

Inserting the result (32) into Eqs. (31) yields finally the set of SRPA equations for the values $\bar{q}^\nu_{sk}$ and $\bar{p}^\nu_{sk}$

$$\begin{aligned} &\sum_{\bar{s}\bar{k}} \{ \bar{q}^\nu_{\bar{s}\bar{k}} [F^{(XX)}_{s'k',\bar{s}\bar{k}} - \kappa^{-1}_{\bar{s}\bar{k},s'k'}] + \bar{p}^\nu_{\bar{s}\bar{k}} F^{(XY)}_{s'k',\bar{s}\bar{k}} \} = 0, \\ &\sum_{\bar{s}\bar{k}} \{ \bar{q}^\nu_{\bar{s}\bar{k}} F^{(YX)}_{s'k',\bar{s}\bar{k}} + \bar{p}^\nu_{\bar{s}\bar{k}} [F^{(YY)}_{s'k',\bar{s}\bar{k}} - \eta^{-1}_{\bar{s}\bar{k},s'k'}] \} = 0, \end{aligned} \quad (33)$$

where

$$F^{(AB)}_{s'k',\bar{s}\bar{k}} = \alpha_{AB} \sum_s \sum_{ph\in s} \frac{1}{\varepsilon^2_{ph} - \omega^2_\nu} \{ \langle ph | \hat{A}^s_{\bar{s}\bar{k}} \rangle^* \langle ph | \hat{B}^s_{s'k'} \rangle \times (\varepsilon_{ph} + \omega_\nu) + \langle ph | \hat{A}^s_{\bar{s}\bar{k}} \rangle \langle \hat{B}^s_{s'k'} | ph \rangle (\varepsilon_{ph} - \omega_\nu) \}, \quad (34)$$

with $A, B \in X, Y$ and

$$\alpha_{AB} = \begin{pmatrix} 1, & \text{for } A = B \\ -i, & \text{for } A = Y, B = X \\ i, & \text{for } A = X, B = Y \end{pmatrix}.$$

The system of linear homogeneous equations (33) has a nontrivial solution only if its determinant is zero. This yields the dispersion equation to obtain the RPA eigenvalues ω_ν.

2. Strength function

When exploring the response of the system to time-dependent external fields, we are often interested in the total strength function rather than in the particular RPA states. For example, giant resonances in heavy nuclei are formed by thousands of RPA states whose contributions in any case cannot be resolved experimentally. In this case, it is more efficient to consider a direct computation of the strength function, which avoids the details and crucially simplifies the calculations.

For an external electric field of multipolarity $E\lambda\mu$, we define the strength function as

$$S_L(\lambda\mu, \omega) = \sum_\nu \omega^L_\nu M^2_{\lambda\mu\nu} \zeta(\omega - \omega_\nu), \quad (35)$$

where $\zeta(\omega - \omega_\nu) = \Delta/[2(\omega - \omega_\nu)^2 + (\Delta/2)^2)]$ is the Lorentz weight with an averaging parameter Δ and $M_{\lambda\mu\nu}$ is the matrix element of $E\lambda\mu$ transition from the ground state to the RPA state $|\nu\rangle$. Unlike the standard definition of the strength function with $\delta(\omega - \omega_\nu)$, we exploit here the Lorentz weight. It is convenient to simulate various smoothing effects.

The strength function (35) can be recast to a form that does not need information on the particular RPA states [41,42]. The explicit derivation is given in [23]. The final expression reads

$$S_L(\lambda\mu, \omega) = \Im \left[\frac{z^L \sum_{\beta\beta'} F_{\beta\beta'}(z) A_\beta(z) A_{\beta'}(z)}{\pi F(z)} \right]_{z=\omega+i\Delta/2} + \sum_s (e^{\rm eff}_s)^2 \sum_{ph\in s} \varepsilon^L_{ph} \langle ph | f_{\lambda\mu} \rangle^2 \zeta(\omega - \varepsilon_{ph}), \quad (36)$$

where $e^{\rm eff}_s$ is an effective charge and $f_{\lambda\mu}$ is the operator of the $E\lambda\mu$ transition. Further, $\Im$ means the image part of the value inside the brackets; $F(z)$ is the determinant of the RPA matrix (33) with ω_ν replaced by the complex argument z; $F_{\beta\beta'}(z)$ is the algebraic supplement of the determinant; and

$$A^{(X)}_{sk}(z) = \sum_{s'} e^{\rm eff}_{s'} \sum_{ph\in s'} \frac{\varepsilon_{ph} \langle ph | X^{s'}_{sk} \rangle \langle ph | f_{\lambda\mu} \rangle}{\varepsilon^2_{ph} - z^2}, \quad (37a)$$

$$A^{(Y)}_{sk}(z) = i \sum_{s'} e^{\rm eff}_{s'} \sum_{ph\in s'} \frac{\omega_\nu \langle ph | Y^{s'}_{sk} \rangle \langle ph | f_{\lambda\mu} \rangle}{\varepsilon^2_{ph} - z^2}. \quad (37b)$$

For the sake of brevity, we introduced in Eq. (36) the new index $\beta = \{skg\}$, where $g = 1$ for time-even and 2 for time-odd quantities. For example, $A_{sk\ g=1} = A^{(X)}_{sk}$ and $A_{sk\ g=2} = A^{(Y)}_{sk}$.

The first term in Eq. (36) collects the contributions of the residual interaction. It vanishes at $V_{\rm res} = 0$. The second term is the unperturbed (purely two-quasiparticle) strength function.

E. Basic features of SRPA

Before proceeding to further specification of the method, it is worth commenting on some of its essential points.

(i) To determine the unknowns $c^{\nu\pm}_{ph,s}$ of a full (nonseparable) RPA, one requires diagonalization of the matrices of a high rank equal to the size of the $1ph$ basis. The separable approximation allows reformulation of the

RPA problem in terms of a few unknowns $\bar{q}_{\bar{k}}$ and $\bar{p}_{\bar{k}}$ and thus reduces dramatically the computational effort. As is seen from Eq. (33), the rank of the SRPA matrix is equal to $4K$ where K is the number of separable operators.

(ii) The number of SRPA states $|\nu\rangle$ is equal to the number of relevant $1ph$ configurations used in the calculations. In heavy nuclei, this number can reach 10^4–10^5. Every state $|\nu\rangle$ is characterized by the particular set of values $\bar{q}^{\nu}_{sk}$ and $\bar{p}^{\nu}_{sk}$.

(iii) Equations (20) and (23) relate the basic SRPA values with the initial functional and input operators $\hat{Q}_{sk}$. After choosing $\hat{Q}_{sk}$, all other SRPA equations are straightforwardly determined following the steps

$$\hat{Q}_{sk} \Rightarrow \langle[\hat{Q}_{sk}, \hat{J}^{\alpha}_{s}]\rangle \Rightarrow \hat{Y}_{sk}, \quad \eta^{-1}_{sk,s'k'} \Rightarrow \hat{P}_{sk} \Rightarrow \langle[\hat{P}_{sk}, \hat{J}^{\alpha}_{s}]\rangle \Rightarrow \hat{X}_{sk}, \quad \kappa^{-1}_{sk,s'k'}. \tag{38}$$

As is discussed in Sec. IV, the proper choice of $\hat{Q}_{sk}$ is crucial to achieve a good convergence of the separable expansion (2) with a minimal number of separable operators. SRPA itself does not provide a recipe to get $\hat{Q}_{sk}$ but these operators can be introduced following intuitive physical arguments.

(iv) SRPA restores the conservation laws (e.g., translational invariance) violated by the static mean field. If a symmetry mode has a generator $\hat{P}_{\rm sym}$, then we keep the conservation law $[\hat{H}, \hat{P}_{\rm sym}] = 0$ by including $\hat{P}_{\rm sym}$ into the set of input generators $\hat{P}_{sk}$ together with its complement $\hat{Q}_{\rm sym} = i[\hat{H}, \hat{P}_{\rm sym}]$.

(v) The basic SRPA operators can be expressed via the separable residual interaction (2) as

$$\hat{X}_{sk} = -i\big[\hat{V}^{\rm sep}_{\rm res}, \hat{P}_{sk}\big]_{ph}, \quad \hat{Y}_{sk} = -i\big[\hat{V}^{\rm sep}_{\rm res}, \hat{Q}_{sk}\big]_{ph}, \tag{39}$$

where the index ph means the $1ph$ part of the commutator. It is seen that the time-odd operator $\hat{P}_{sk}$ retains the time-even part of $V^{\rm sep}_{\rm res}$ to build $\hat{X}_{sk}$. Vice versa, the commutator with the time-even operator $\hat{Q}_{sk}$ keeps the time-odd part of $V^{\rm sep}_{\rm res}$ to build $\hat{Y}_{sk}$.

III. SRPA WITH THE SKYRME FUNCTIONAL

A. Skyrme functional

We use the Skyrme functional [24] in the form [25,26,38]

$$E = \int d\vec{r}(\mathcal{H}_{\rm kin} + \mathcal{H}_{\rm Sk}(\rho_s, \tau_s, \vec{\sigma}_s, \vec{j}_s, \vec{\Im}_s) + \mathcal{H}_{\rm pair}(\chi_s) + \mathcal{H}_{\rm C}(\rho_p)), \tag{40}$$

where

$$\mathcal{H}_{\rm kin} = \frac{\hbar^2}{2m}\tau, \tag{41}$$

$$\mathcal{H}_{\rm Sk} = \frac{b_0}{2}\rho^2 - \frac{b'_0}{2}\sum_s \rho_s^2 - \frac{b_2}{2}\rho(\Delta\rho) + \frac{b'_2}{2}\sum_s \rho_s(\Delta\rho_s) + \frac{b_3}{3}\rho^{\alpha+2} - \frac{b'_3}{3}\rho^{\alpha}\sum_s \rho_s^2 + b_1(\rho\tau - \vec{j}^2) - b'_1\sum_s\left(\rho_s\tau_s - \vec{j}_s^2\right) - b_4(\rho(\vec{\nabla}\vec{\Im}) + \vec{\sigma}\cdot(\vec{\nabla}\times\vec{j})) - b'_4\sum_s(\rho_s(\vec{\nabla}\vec{\Im}_s) + \vec{\sigma}_s\cdot(\vec{\nabla}\times\vec{j}_s)), \tag{42}$$

$$\mathcal{H}_{\rm pair}(\chi_s) = \frac{1}{2}\sum_s V_{{\rm pair},s}\chi_s^*\chi_s, \tag{43}$$

$$\mathcal{H}_{\rm C} = \frac{e^2}{2}\int d\vec{r}_1\rho_p(\vec{r})\frac{1}{|\vec{r}-\vec{r}_1|}\rho_p(\vec{r}_1) - \frac{3}{4}e^2\left(\frac{3}{\pi}\right)^{\frac{1}{3}}[\rho_p(\vec{r})]^{\frac{4}{3}}, \tag{44}$$

are kinetic, Skyrme, pairing, and Coulomb terms, respectively. The densities and currents used in this functional are defined in the Appendices A and C. Densities without the index s involve both neutrons and protons, e.g., $\rho = \rho_p + \rho_n$. Parameters b_i and α are fitted to describe ground state properties of atomic nuclei (see, e.g., Ref. [1]).

For the sake of brevity, we omit here the derivation of the Skyrme mean field, which can be found elsewhere, e.g., in Refs. [19,23,38], and present only the main values entering the SRPA equations.

B. Second functional derivatives

The crucial ingredients of the Skyrme SRPA residual interaction are the second functional derivatives entering expressions for the basic operators (20) and strength matrices (23). They read

$$\frac{\delta^2 E}{\delta\rho_{s_1}(\vec{r}_1)\delta\rho_s(\vec{r})} = b_0 - b'_0\delta_{ss_1} - (b_2 - b'_2\delta_{ss_1})\Delta_{\vec{r}_1} + b_3\frac{(\alpha+2)(\alpha+1)}{3}\rho^{\alpha}(\vec{r}) - b'_3\left[\frac{\alpha(\alpha-1)}{3}\rho^{\alpha-2}(\vec{r})\sum_{s_2}\rho_{s_2}^2(\vec{r}) + \frac{2\alpha}{3}\rho^{\alpha-1}(\vec{r})(\rho_s(\vec{r}) + \rho_{s_1}(\vec{r})) + \delta_{ss_1}\frac{2}{3}\rho^{\alpha}(\vec{r})\right] - \delta_{ss_1}\delta_{sp}\frac{1}{3}\left(\frac{2}{\pi}\right)^{1/3} \times [\rho_p(\vec{r})]^{-2/3}\}\,\delta(\vec{r}-\vec{r}_1) + \delta_{ss_1}\delta_{sp}\frac{e^2}{|\vec{r}-\vec{r}_1|}, \tag{45}$$

$$\frac{\delta^2 E}{\delta\tau_{s_1}(\vec{r}_1)\delta\rho_s(\vec{r})} = [b_1 - b'_1\delta_{ss_1}]\delta(\vec{r}-\vec{r}_1), \tag{46}$$

$$\frac{\delta^2 E}{\delta\vec{\Im}_{s_1}(\vec{r}_1)\delta\rho_s(\vec{r})} = [b_4 + b'_4\delta_{ss_1}]\vec{\nabla}_{\vec{r}_1}\delta(\vec{r}-\vec{r}_1), \tag{47}$$

$$\frac{\delta^2 E}{\delta\rho_{s_1}(\vec{r}_1)\delta\vec{\Im}_s(\vec{r})} = -[b_4 + b'_4\delta_{ss_1}]\vec{\nabla}_{\vec{r}_1}\delta(\vec{r}-\vec{r}_1) \tag{48}$$

for time-even densities and

$$\frac{\delta^2 E}{\delta j_{s_1,m}(\vec{r}_1)\delta j_{s,n}(\vec{r})} = 2[-b_1 + b_1'\delta_{ss_1}]\delta_{mn}\delta(\vec{r}_1 - \vec{r}), \tag{49}$$

$$\frac{\delta^2 E}{\delta \sigma_{s_1,m}(\vec{r}_1)\delta j_{s,n}(\vec{r})} = -[b_4 + b_4'\delta_{ss_1}]\epsilon_{mnl}\nabla_{\vec{r}_1,\,l}\delta(\vec{r}_1 - \vec{r}) \tag{50}$$

for time-odd densities. The last two terms in Eq. (45) represent the exchange and direct Coulomb contributions. Further, the indices m and n in Eqs. (49) and (50) run over the three basis spatial directions of the chosen representation (in our case the cylindrical coordinate system) and ϵ_{mnl} is the totally antisymmetric tensor associated with the vector product.

C. Presentation via matrix elements

The responses in Eqs. (20) and (23) are expressed in terms of the averaged commutators

$$\langle[\hat{A}, \hat{B}]\rangle \quad \text{with} \quad \gamma_T^A = -\gamma_T^B, \tag{51}$$

where $|\,\rangle$ is the quasiparticle vacuum. Calculation of these values can be considerably simplified if expressing them through the matrix elements of the operators $\hat{A}$ and $\hat{B}$.

To be specific, we associate the operator $\hat{A}$ with a time-even operator $\hat{Q}$ or a time-odd operator $\hat{P}$, which have real or imaginary matrix elements, respectively. Then

$$\langle[\hat{Q}_{sk}, \hat{B}_s]\rangle = 4i \sum_{ph\in s} \langle ph|\hat{Q}_{sk}\rangle \Im\langle ph|\hat{B}_s\rangle, \tag{52a}$$

$$\langle[\hat{P}_{sk}, \hat{B}_s]\rangle = -4 \sum_{ph\in s} \langle ph|\hat{P}_{sk}\rangle \Re\langle ph|\hat{B}_s\rangle, \tag{52b}$$

where both p and h run over all single-particle states and $\Im$ and $\Re$ mean the imaginary and real parts of the values to the right. The pairing factors are included in the single-particle matrix elements.

Then elements of the inverse strength matrices are real and read

$$\kappa^{-1}_{s'k',sk} = -i\langle[\hat{P}_{s'k'}, \hat{X}^{s'}_{sk}]\rangle = 4i \sum_{ph\in s'} \langle ph|\hat{P}_{s'k'}\rangle\, \Re\langle ph|\hat{X}^{s'}_{sk}\rangle, \tag{53a}$$

$$\eta^{-1}_{s'k',sk} = -i\langle[\hat{Q}_{k'}, \hat{Y}_k\rangle = 4 \sum_{ph\in s'} \langle ph|\hat{Q}_{s'k'}\rangle\, \Im\langle ph|\hat{Y}^{s'}_{sk}]\rangle. \tag{53b}$$

The responses entering $\hat{X}$ and $\hat{Y}$ in Eq. (20) are also real and read

$$\mathcal{R}^{\alpha}_{X,sk} = i\langle[\hat{P}_{sk}, \hat{J}^{\alpha}_s]\rangle = -4i \sum_{ph\in s} \langle ph|\hat{P}_{sk}\rangle\, \Re\langle ph|\hat{J}^{\alpha}_s\rangle, \tag{54a}$$

$$\mathcal{R}^{\alpha}_{Y,sk} = i\langle[\hat{Q}_{sk}, \hat{J}^{\alpha}_s]\rangle = -4 \sum_{ph\in s} \langle ph|\hat{Q}_{sk}\rangle\, \Im\langle ph|\hat{J}^{\alpha}_s\rangle, \tag{54b}$$

where $\langle ph|\hat{J}^{\alpha}_s|\rangle$ are transition densities.

We actually deal with axially symmetric systems. The modes then can be sorted into channels with a given angular-momentum projection μ to the symmetry axis z. For even-even nuclei μ takes integer values. The explicit expressions for the responses in cylindrical coordinates (see definition of these coordinates in Appendix B) then read

$$\begin{aligned}\vec{j}_{Y,sk}(\vec{r}) &= i\langle[\hat{Q}_{sk}, \hat{\vec{j}}_s]\rangle \\ &= \big(\vec{e}_\rho j^{\rho}_{Y,sk}(\rho, z) + \vec{e}_z j^{z}_{Y,sk}(\rho, z)\big)\cos\mu\theta \\ &\quad + \vec{e}_\theta j^{\theta}_{Y,sk}(\rho, z)\sin\mu\theta,\end{aligned} \tag{55}$$

$$\begin{aligned}\vec{s}_{Y,sk}(\vec{r}) &= i\langle[\hat{Q}_{sk}, \hat{\vec{s}}_s]\rangle \\ &= \big(\vec{e}_\rho s^{\rho}_{Y,sk}(\rho, z) + \vec{e}_z s^{z}_{Y,sk}(\rho, z)\big)\sin\mu\theta \\ &\quad + \vec{e}_\theta s^{\theta}_{Y,sk}(\rho, z)\cos\mu\theta,\end{aligned} \tag{56}$$

$$\rho_{X,sk}(\vec{r}) = i\langle[\hat{P}_{sk}, \hat{\rho}_s]\rangle = \rho_{X,sk}(\rho, z)\cos\mu\theta, \tag{57}$$

$$\tau_{X,sk}(\vec{r}) = i\langle[\hat{P}_{sk}, \hat{\tau}_s]\rangle = \tau_{X,sk}(\rho, z)\cos\mu\theta, \tag{58}$$

$$\begin{aligned}\vec{\Im}_{X,sk}(\vec{r}) &= i\langle[\hat{P}_{sk}, \hat{\vec{\Im}}_s]\rangle \\ &= \big(\vec{e}_\rho \Im^{\rho}_{X,sk}(\rho, z) + \vec{e}_z \Im^{z}_{X,sk}(\rho, z)\big)\cos\mu\theta \\ &\quad + \vec{e}_\theta \Im^{\theta}_{X,sk}(\rho, z)\sin\mu\theta,\end{aligned} \tag{59}$$

where $\{\rho, z\}$-depending response components are real. All the dependence on the spatial coordinates follows from the transition densities entering the responses.

The response components involving $\sin\mu\theta$ obviously vanish for modes with $\mu = 0$.

Explicit expressions in cylindrical coordinates for strength matrices, responses, transition densities, matrix elements, Coulomb contributions, and other SRPA values can be found in Ref. [23]. It is to be noted that the present calculations do not yet include the Coulomb contribution to the residual interaction. This introduces the uncertainty reaching up to $\sim$0.4 MeV in an average peak position [43]. Such effect is safely below the precision of the present investigation.

IV. CHOICE OF INITIAL OPERATORS

As was mentioned in Sec. II E, SRPA starts with the choice of appropriate generating operators $\hat{Q}_{sk}$; see the sequence of the model steps in Eq. (38). The SRPA formalism itself does not provide these operators. At the same time, their proper choice is crucial to get good convergence of the separable expansion (2) with a minimal number of separable terms. The choice should be simple and universal in the sense that it can be applied equally well to different modes and excitation channels.

We propose a choice inspired by physical arguments. The main idea is that the generating operators should explore different spatial regions of the nucleus, the surface as well as the interior. The leading scaling generator should have the form of the applied external field in the long-wave approximation, which is most sensitive to the surface of the system. Since nuclear collective motion dominates in the surface region, already this generator should provide a good description. Next, generators should be localized more in the interior to describe an interplay of surface and volume vibrations. For $E\lambda$ giant resonances in spherical nuclei, we used a set of generators with the radial dependencies in the form of power and Bessel functions [19]. In the present study for deformed nuclei, we

implement, for the sake of simplicity, only generators with the power radial dependence

$$\hat{Q}_k(\vec{r}) = r^{\lambda+2(k-1)}(Y_{\lambda\mu}(\Omega) + h.c.). \quad (60)$$

The separable operators $\hat{X}_k$ and $\hat{Y}_k$ with $k = 1$ are mainly localized at the nuclear surface while the operators with $k > 1$ are allowed to touch, at least partly, the nuclear interior. This simple set seems to be a good compromise for the first calculations of the giant resonances. Our analysis shows that already two first operators with $k = 1, 2$ suffice for a spectral resolution of 2 MeV, as discussed below. In the next studies we plan to enlarge the list of the input generators so as to cover properly the nuclear interior and to take into account the coupling of the modes with different λ, induced by the deformation.

V. RESULTS AND DISCUSSION

A. Aims and details of calculations

The main aim of the present calculations is to demonstrate the ability of SRPA to describe multipole giant resonances (GR) in deformed nuclei and to explore the dependence of the resonance strength distributions on the nuclear matter properties and some terms of the Skyrme functional. The isovector giant dipole resonance (GDR) and isoscalar giant quadrupole resonance (GQR) in the axially deformed nuclei ^{154}Sm, ^{238}U, and ^{254}No are considered. We employ a representative set of Skyrme forces, SkT6 [33], SkM* [34], SLy6 [35], and SkI3 [36], with different features (isoscalar and isovector effective masses, asymmetry energy, etc.). These forces are widely used for the description of ground state properties and dynamics of atomic nuclei [1] including deformed ones. As is seen from Table I, the forces span a variety of nuclear matter properties while all correctly reproducing experimental values of the quadrupole moments in ^{154}Sm and ^{238}U.

The calculations use a cylindrical coordinate-space grid with a spacing of 0.7 fm. Pairing is treated at the BCS level and is frozen in the dynamical calculations. The collective response for the GDR ($\lambda = 1$) and GQR ($\lambda = 2$) is computed with two input operators (60) at $k = 1$ and 2. Both GR are calculated in terms of the energy-weighted ($L = 1$) strength function (36)

TABLE I. Nuclear matter and deformation properties for the Skyrme forces under consideration. The table represents the isoscalar effective mass m_0^*/m, symmetry energy $a_{\rm sym}$, sum rule enhancement factor κ, isovector effective mass $m_1^*/m = 1/(1+\kappa)$, and quadrupole moments Q_2 in ^{154}Sm, ^{238}U, and ^{254}No. Experimental values of the quadrupole moment in ^{154}Sm and ^{238}U are 6.6 and 11.1 b, respectively [44].

Forces	m_0^*/m	$a_{\rm sym}$ (MeV)	κ	m_1^*/m	Q_2 [b]		
					^{154}Sm	^{238}U	^{254}No
SkT6	1.00	30.0	0.001	1.00	6.8	11.1	13.7
SkM*	0.79	30.0	0.531	0.65	6.8	11.1	14.0
SLy6	0.69	32.0	0.250	0.80	6.8	11.0	13.7
SkI3	0.58	34.8	0.246	0.80	6.8	11.0	13.7

with the averaging parameter $\Delta = 2$ MeV (as most suitable for the comparison with the experiment). The factorization of the residual interaction and the strength function technique dramatically reduce the computational effort. For example, by using a PC with CPU Pentium 4 (3.0 GHz) we need about 25 min for the complete calculations of the GDR in ^{238}U, including 1 min for computation of the strength function itself.

The isovector GDR and isoscalar GQR are calculated with the effective charges $e_p^{\rm eff} = N/A$, $e_n^{\rm eff} = -Z/A$, and $e_p^{\rm eff} = e_n^{\rm eff} = 1$, respectively. The isoscalar dipole spurious mode is located at 2–3 MeV. The deviation from the desirable zero energy is caused by several reasons. First, we have neglected in the present study the contribution from the Coulomb residual interaction. The second (more important) reason is that the nucleus is treated in a finite coordinate box, which artificially binds the center of mass. Larger numerical boxes could help here but at quickly increasing computational cost. In any case, it suffices for our present purposes that the center-of-mass mode lies at a low energy and thus is safely separated from the GDR.

We use a large configuration space including the single-particle spectrum from the bottom of the potential well up to $\sim +16$ MeV. This results in 7000–10000 dipole and 11000–17000 quadrupole two-quasiparticle configurations in the energy interval 0–100 MeV. The relevant energy-weighted sum rules are exhausted by 85%–95%. Such a basis is certainly enough for the present aims.

B. Discussion of results

Results of the calculations are presented in Figs. 1–3. The first two figures compare the calculated GDR and GQR with the available photoabsorption [45,46] and (α, α') [47] experimental data. It is seen that all four Skyrme forces provide in general an appropriate agreement with the experiment. So, SRPA indeed can give a robust treatment of the multipole GR and, what is important, does this with minimal computational effort.

To illustrate the accuracy of the method, we give for ^{254}No the strength functions calculated with one ($k = 1$) and two ($k = 1, 2$) input operators. It is seen that both cases are about equal for the GQR with its simple one-bump structure. At the same time, the second operator considerably changes the gross structure of the more complicated GDR. We have checked that inclusion of more operators ($k \geqslant 3$) does not result in further significant modification of the GDR. So, the approximation of two input operators seems to be reasonable, at least for the present study at a resolution of 2 MeV.

The figures also show the unperturbed strengths, i.e., the mere two-quasiparticle ($2qp$) distributions without the residual interaction. Comparison of these strengths with the fully coupled collective strengths (solid curves) displays the collective E1 and E2 shifts. As a trivial fact, we observe the proper right shift for the isovector GDR and the left shift for the isoscalar GQR. What is more interesting, the shifts for both resonances (including isovector DGR) depend on the *isoscalar* effective mass m_0^*/m. To explain this, one should remember that the smaller the m_0^*/m, the more stretched

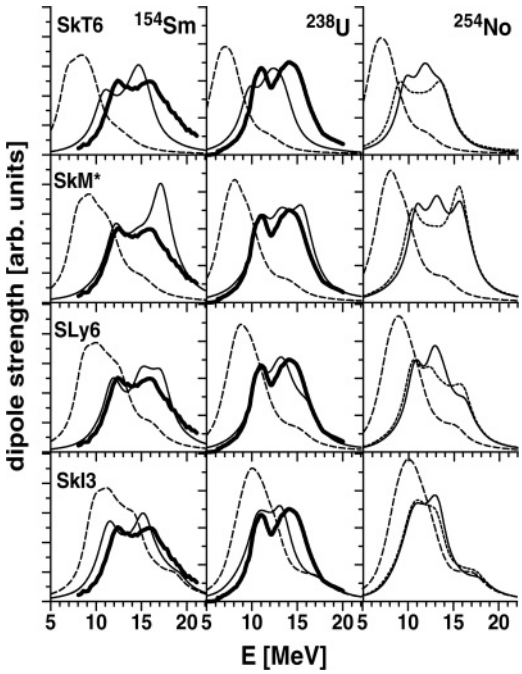

FIG. 1. The isovector GDR in ^{154}Sm, ^{238}U, and ^{254}No calculated with the Skyrme forces SkT6, SkM*, SLy6, and SkI3. The plots depict the collective strength calculated with two (solid curve) and one (dotted curve for ^{254}No) input operators, the unperturbed quasiparticle strength (dashed curve), and the photoabsorption experimental data [45,46] (bold curve consisting of triangles) for ^{238}U and ^{254}No.

the single-particle spectrum [1] (see also relevant examples in [48]). And indeed the E1 and E2 unperturbed strengths in the figures exhibit a systematic shift to higher energy while moving from SkT6 to SkI3 (for E1 the shift is essentially weaker than for E2 [49]). Simultaneously, we have the corresponding evolution of the collective energy shifts. Namely, they decrease for GDR and increase for GQR (with the exception of GDR for SkT6). All these trends lead to a remarkable net result: strong variations of the unperturbed strengths and collective shifts with m_0^*/m considerably compensate each other so that the final GDR and GQR energies become much less sensitive to different Skyrme forces and approach the experimental values.

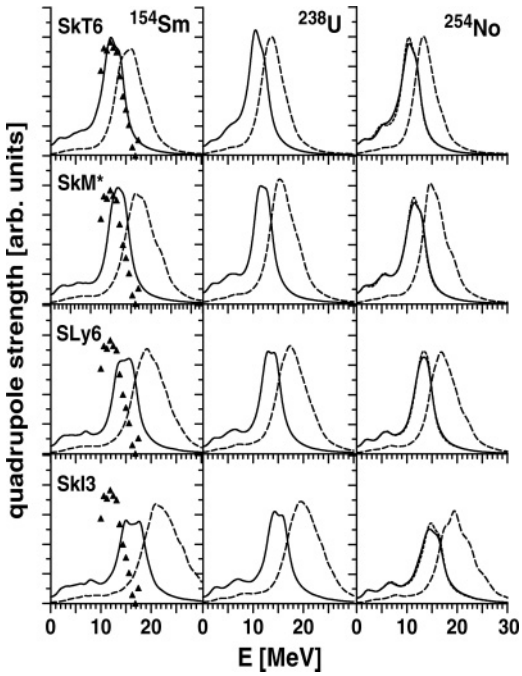

FIG. 2. The same as in Fig. 1 but for isoscalar GQR and (α, α') experimental data [47] (triangles) for ^{154}Sm.

The remaining energy differences of order $\sim$1 MeV show some other, sometimes known, trends for the GR.

First, we see a systematic (with the exception of SkT6) downshift of the calculated GDR with increasing symmetry energy $a_{\rm sym}$. This, at first glance, surprising result complies with the experience of the systematic studies in spherical nuclei [50]. The case of SkT6 looks to be the exception to this simple rule. It has the same asymmetry energy as SkM* (see Table I) but a lower GDR resonance peak. This happens because the density dependence $da_{\rm sym}/d\rho$ is abnormally low here (for reasons whose discussion goes beyond the scope of the present article). In addition to the trend with $a_{\rm sym}$, Fig. 1 also hints a connection of the GDR energy with the sum rule enhancement factor κ and the related value of the *isovector* effective mass m_1^*/m. Namely, the smaller the effective mass (larger the κ), the higher the GDR. The trends and connections mentioned above should, however, be considered with a bit of care. Indeed, the variation of $a_{\rm sym}$ between the different Skyrme forces in Table I is rather small and probably not enough to demonstrate a strong and unambiguous trend. Moreover, a complicated dependence of GDR on *different* isovector factors can spoil and entangle the concrete trends. In any case, analysis of the DGR trends deserves more systematic study that is now in reach with the efficient SRPA technique.

Instead, the evolution of isoscalar GQR is more clear and systematic. We see a steady upshift of the GQR peak from SkT6* to SkI3, which complies with the known dependence on the isoscalar effective mass m_0^*/m [51]; namely, the lower the effective mass, the higher the GQR. This trend has a simple explanation. As discussed previously, the low m_0^*/m results in stretching the single-particle spectrum and thus in the upshift of the $2qp$ quadrupole strength. In the GQR case, the opposite dependence of the collective shift is not enough to compensate the strong $2qp$ upshift and hence we obtain the trend. Note that in our calculations SkT6 with $m_0^*/m = 1$ yields the best agreement for the GQR. This confirms to some extend the findings [51] for ^{208}Pb that a good reproduction of the GQR requires a large effective mass.

The shape and width of GR in deformed nuclei are mainly determined by the deformation splitting and the spectral fragmentation due to interference with energetically close $1ph$ states (Landau fragmentation). Following Table I, the different Skyrme forces provide quite similar quadrupole moments. Hence they result in close deformation splittings. Instead, the Landau fragmentation depends sensitively on the spectral pattern of a model, determined to a large extent by isoscalar and isovector effective masses. Our samples of forces contain sufficient variation of both ones. Nonetheless, it turns out that

the width and shape of the GQR are practically the same for all the four Skyrme forces.

At the same time, the strongest variation is found for the GDR whose width and gross structure significantly depend on the force. It is seen that SkM* gives an artificial right shoulder (especially in ^{154}Sm) and thus an overestimation of the GDR width. This effect weakens for SLy6 (leading to the best description of GDR) and vanishes completely for SkI3 (resulting in underestimation of the resonance width). The appearance of the artificial right shoulder for SkM* and SLy6 has already been noted for deformed rare-earth and actinide nuclei [4] and ^{208}Pb [19]. For the particular Skyrme forces, this effect seems to be universal. It takes place for GDR in heavy nuclei, independently of their shape. As is shown in Ref. [52], the right shoulder is provoked by an excessive collective shift and further enforced by the presence in the region of the $2qp$ bunch composed from the particular high-moment configurations ($\pi 1g_{9/2}$ and $\nu 1h_{11/2}$ for ^{154}Sm and $\pi 1h_{11/2}$ and $\nu 1i_{13/2}$ for ^{238}U and ^{254}No) [52]. These configurations represent the intruder $l + 1/2$ states entering the valence shell due to the strong spin-orbital splitting. They form a dense $2qp$ bunch that is easily excited and thus provides high sensitivity of the right GDR flank. This feature can be useful for additional selection of the parameters of Skyrme forces.

It would be very interesting to relate the above results for the GDR width and profile with the effective masses. Some possible correlations can immediately be noted. For example, the evolution of the right shoulder from SkM* to SkI3 seems to correlate with a systematic decrease of m_0^*/m. Moreover, the largest right shoulder in SkM* can be related with the smallest value of m_1^*/m for this force. These connections, however, require further confirmation from more extended studies with an even broader basis of forces. In any case, the results hint that the properties of the isovector GDR probably depend not only on the isovector m_1^*/m but also on the isoscalar m_0^*/m. At first glance, this statement looks surprising. However, we should take into account that m_0^*/m influences the mean level spacings $\bar{\epsilon}$ in the mean field and, hence, can in principle affect the GDR. The resonance should depend on the ground state properties which in turn are related to m_0^*/m. It also worth noting that both m_0^*/m and m_1^*/m are generated by one and the same term of the Skyrme functional ($\sim b_1, b_1'$) and so probably are not fully decoupled in the dynamics. Some nontrivial relations between isoscalar and isovector parameters are already discussed in literature, e.g., the relation $\bar{\epsilon} m_0^*/m \approx \kappa m_1^*/m$ and its connection with $a_{\rm sym}$ [53]. And we see here an interesting field for future investigations.

As a next step, let's consider contributions of the time-odd densities to the GDR and GQR. These results are illustrated in Fig. 3. The calculations show that only the current-current contribution (49) is essential whereas the contribution (50) connected with the spin density is negligible. So, in Fig. 3 we display only the effect of the current density. First of all, it is worth noting that the most significant changes appear again at the right flank of the resonances. Probably, the high-moment $l + 1/2$ configurations mentioned previously play an important role not only for GDR but also for GQR.

The impact of the time-odd current is different in GDR and GQR. In the quadrupole resonance, we see the systematic

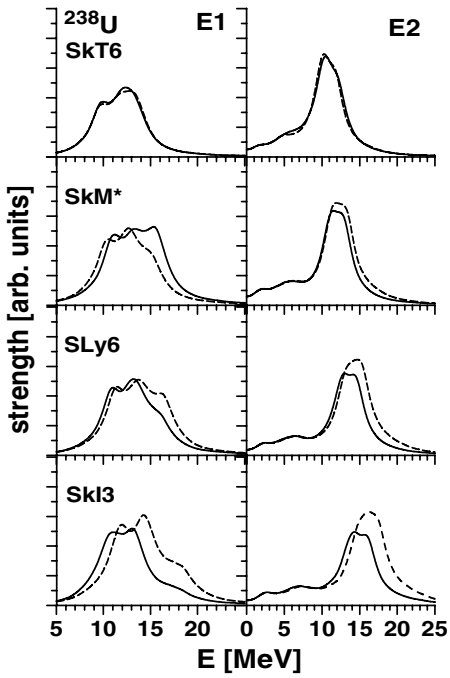

FIG. 3. The isovector GDR and isoscalar GQR in ^{238}U calculated with the Skyrme forces SkT6, SkM*, SLy6, and SkI3. The strength is calculated with (solid curve) and without (dashed curve) the contribution of the time-odd current.

downshift and narrowing of the strength. There is a clear correlation with the value of the isoscalar effective mass: the lower the m_0^*/m, the stronger the time-odd effect. After inclusion of the time-odd coupling, the GQR for different m_0^*/m become much closer. So, the time-odd contribution weakens the influence of m_0^*/m.

In the dipole resonance, the time-odd shift is not so systematic. We observe no shift for SkT6, the upshift for SkM*, and the downshifts for SLy6 and SkI3. Again one may note some correlation with effective masses. The specific SkM* case can be connected with very small m_1^*/m for this force. Moreover, one may note (with the exception of SkM*) increasing the time-odd impact with lowering m_0^*/m. In principle, the correlations between the influence of time-odd terms and effective masses in both GDR and GQR cases were more or less expected because the current density enters the term of the Skyrme functional $\sim b_1, b_1'$ just responsible for generation of the effective masses. This explains why the SkT6 case with $m_0^*/m = m_1^*/m = 1$ (no effective mass effects) does not demonstrate any time-odd impact.

It is worth noting that the dominant contributions to the collective response from the principle terms of the Skyrme functional have different signs and, thus, to a large extent, compensate each other (this can be easily checked in the SRPA by estimation of the different contributions to the inverse strength constants (23). As a result, the smaller contributions (time-odd, spin-orbital, and Coulomb) become important.

The present study involves three nuclei from different mass regions and four Skyrme forces with various bulk properties. We have yet to disentangle more carefully the separate influences of them. This requires systematic variations of forces

in a large set of test cases. Because of the computationally efficient SRPA method, such systematic studies can now be easily performed.

VI. CONCLUSIONS

A general procedure for the self-consistent factorization of the residual nuclear interaction is proposed for arbitrary density- and current-dependent functionals. Following this procedure, the SRPA method is derived. SRPA dramatically simplifies the calculations while providing a reliable description of nuclear excitations. The reduction of the computational effort is especially useful for deformed nuclei. In the present article, SRPA with Skyrme forces is specified for the description of collective dynamics in axially deformed nuclei.

For the first explorations, SRPA is applied for description of isovector giant dipole resonances (GDR) and isoscalar giant quadrupole resonances (GQR) in deformed nuclei from rare-earth (^{154}Sm), actinide (^{238}U), and superheavy (^{254}No) regions. Four Skyrme forces (SkT6, SkM*, SLy6, and SkI3) with essentially different bulk properties are used. The calculations show that SRPA can successfully describe multipole giant resonances. A good agreement with available experimental data is achieved, especially with SLy6 for GDR. We did not find any peculiarities of the GR in superheavy nuclei. The behavior of the resonances in all three mass regions looks quite similar.

We analyzed dependence of GDR and GQR descriptions on various Skyrme forces, in particular on the isoscalar and isovector effective masses and the symmetry energy. The contribution of the time-odd couplings was also explored. Some known trends for GDR with $a_{\rm sym}$ and GQR with m_0^*/m were reproduced. Moreover, the close relation between the time-odd contribution and m_0^*/m was demonstrated for GQR. The calculations also hint at some interesting (though not enough systematic) trends for GDR. Altogether, the results point out correlations between isoscalar and isovector masses and time-odd contributions. The correlation seem to be natural because all the items originate from one and the same term of the Skyrme functional.

The time-odd and effective mass impacts manifest themselves mainly at the right flanks of the strength distributions. The impacts are much stronger and diverse for GDR. Moreover, this resonance exhibits the strong Landau fragmentation. The GDR gross structure considerably depends on the applied Skyrme force and the related effective masses. As a result, the GDR structure can serve as an additional test for selection of the Skyrme parameters and related nuclear matter values.

ACKNOWLEDGMENTS

This work is part of the research plan MSM 0021620834 supported by the Ministry of Education of the Czech Republic. It was partly funded by the Czech grant agency (Grant 202/06/0363) and the grant agency of Charles University in Prague (Grant 222/2006/B-FYZ/MFF). We are thankful for the support from DFG Grant GZ:436 RUS 17/104/05 and Heisenberg-Landau (Germany-BLTP JINR) grants for the years 2005 and 2006. W.K. and P.-G.R. are grateful for the BMBF support under Contracts 06 ER 808 and 06 DD 119.

APPENDIX A: DENSITY OPERATORS FOR SKYRME FUNCTIONAL

In our study the Skyrme forces include time-even (spatial, kinetic-energy, spin-orbit) and time-odd (current, spin) densities associated with the hermitian operators

$$\hat{\rho}_s(\vec{r}) = \sum_{i=1}^{N_s} \delta(\vec{r}_i - \vec{r}),$$

$$\hat{\tau}_s(\vec{r}) = \sum_{i=1}^{N_s} \overleftarrow{\nabla}\delta(\vec{r}_i - \vec{r})\vec{\nabla},$$

$$\hat{\vec{\Im}}_s(\vec{r}) = \sum_{i=1}^{N_s} \delta(\vec{r}_i - \vec{r})\vec{\nabla}\times\hat{\vec{\sigma}},$$

$$\hat{\vec{j}}_s(\vec{r}) = \frac{1}{2}\sum_{i=1}^{N_s}\{\vec{\nabla}, \delta(\vec{r}_i - \vec{r})\},$$

$$\hat{\vec{\sigma}}_s(\vec{r}) = \sum_{i=1}^{N_s} \delta(\vec{r}_i - \vec{r})\hat{\vec{\sigma}}.$$

where $\hat{\vec{\sigma}}$ is the Pauli matrix and N_s is the number of protons or neutrons.

The densities read as

$$J_s^\alpha(\vec{r}) = \sum_{j\in s} v_j^2 \varphi_j^*(\vec{r})\hat{J}_s^\alpha \varphi_j(\vec{r}), \tag{A1}$$

where $\hat{J}_s^\alpha$ is the density operator, $\varphi_j(\vec{r})$ is the wave function of the single-particle state j, and v_j^2 is the pairing occupation weight.

APPENDIX B: WAVE FUNCTION IN CYLINDRICAL COORDINATES

Cylindrical coordinates ρ, z, θ are defined as

$$x = \rho\cos\vartheta, \quad y = \rho\sin\vartheta, \quad z = z.$$

Then the single-particle particle wave function and its time reversal have the form of spinors

$$\varphi_j(\vec{r}) = \begin{pmatrix} R_j^{(+)}(\rho, z)e^{im_j^{(+)}\vartheta} \\ R_j^{(-)}(\rho, z)e^{im_j^{(-)}\vartheta} \end{pmatrix}, \tag{B1}$$

$$\varphi_{\bar{j}}(\vec{r}) = \hat{T}\varphi_j(\vec{r}) = \begin{pmatrix} -R_j^{(-)}(\rho, z)e^{-im_j^{(-)}\vartheta} \\ R_j^{(+)}(\rho, z)e^{-im_j^{(+)}\vartheta} \end{pmatrix}, \tag{B2}$$

where K_j is the projection of the complete single-particle moment onto symmetry z axis of the axial nucleus.

Expressions for differential operators in cylindrical coordinates are elsewhere (see, e.g., Ref. [54]).

APPENDIX C: PAIRING CONTRIBUTION

The pairing is treated with the Bardin-Coopper-Schriffer (BCS) method. Then the SRPA values gain the pairing factors involving coefficients v_j and u_j of the Bogoliubov transformation from particles to quasiparticles.

The densities and currents in the Skyrme functional dominate in the particle-hole channel. The pairing density falls into another channel provided by the two-particle excitations. It involves a different pairing weight, namely, $u_j v_j$, rather than the v_j^2 for the standard densities (A1). Specifically the pairing density reads

$$\chi_s = \sum_{j\in s} u_j v_j |\varphi_j|^2. \tag{C1}$$

In the case of pairing, the hermitian one-body operators with a given time-parity ($\gamma_T^A = 1$, $\gamma_T^B = -1$) obtain in the *ph* channel the form

$$\hat{A} = 2\sum_{ij}\langle ij|A\rangle u_{ij}^{(+)}(\hat{A}_{ij}^{\dagger} + \hat{A}_{ij}), \tag{C2}$$

$$\hat{B} = 2\sum_{ij}\langle ij|B|\rangle u_{ij}^{(-)}(\hat{A}_{ij}^{\dagger} + \hat{A}_{ij}), \tag{C3}$$

where

$$\hat{A}_{ij}^{\dagger} = \hat{\alpha}_i^{\dagger}\hat{\alpha}_{\bar{j}}^{\dagger}, \quad \hat{A}_{ij} = \hat{\alpha}_{\bar{j}}\hat{\alpha}_i \tag{C4}$$

are two-quasiparticle operators and

$$u_{ij}^{(+)} = u_i v_j + u_j v_i, \quad u_{ij}^{(-)} = u_i v_j - u_j v_i \tag{C5}$$

are the pairing factors. This is the case for time-even operators $\hat{Q}_{sk}$ and $\hat{X}_{sk}$ and the time-odd operator $\hat{Y}_{sk}$. The time-odd operators

$$\begin{aligned}\hat{P}_{sk} &= i[\hat{H}, \hat{Q}_{sk}] = i\left\{[\hat{h}_0, \hat{Q}_{sk}] + \left[\hat{V}_{\rm res}^{\rm sep}, \hat{Q}_{sk}\right]\right\} \\ &= i[\hat{h}_0, \hat{Q}_{sk}] - \hat{Y}_{sk}\end{aligned} \tag{C6}$$

have a more complicated form because of the additional term $i[\hat{h}_0, \hat{Q}_{sk}]$. Namely, it reads

$$\hat{P}_{sk} = 2\sum_{ij\epsilon s}\left\{i2\epsilon_{ij}u_{ij}^{(+)}\langle ij|Q_{sk}\rangle - u_{ij}^{(-)}\langle ij|Y_{sk}^{s}\rangle\right\}\cdot(\hat{A}_{ij}^{\dagger} - \hat{A}_{ij}). \tag{C7}$$

The SRPA formalism in Secs. II and III is presented in a general form equally suitable for cases with and without pairing. In the case of pairing, the ground and perturbed 1*ph* many-body wave functions are replaced by their BCS counterparts, the summation indices p and h run the quasiparticle states, and the involved values (densities, operators, and matrix elements) acquire the pairing factors given above.

The pairing is not important for giant resonances considered in the present study. So, we freeze the pairing in the dynamics and do not present here the explicit form of the pairing contribution (pairing vibrations) to the residual interaction. Some examples of this contribution can be found in Ref. [23].

[1] M. Bender, P.-H. Heenen, and P.-G. Reinhard, Rev. Mod. Phys. **75**, 121 (2003).
[2] M. V. Stoitsov, J. Dobaczewski, W. Nazarewicz, S. Pittel, and D. J. Dean, Phys. Rev. C **68**, 054312 (2003).
[3] A. Obertelli, S. Peru, J. P. Delaroche, A. Gillibert, M. Girod, and H. Goutte, Phys. Rev. C **71**, 024304 (2005).
[4] J. A. Maruhn, P.-G. Reinhard, P. D. Stevenson, J. R. Stone, and M. R. Strayer, Phys. Rev. C **71**, 064328 (2005).
[5] J. Terasaki, J. Engel, M. Bender, J. Dobaczewski, W. Nazarewicz, and M. Stoitsov, Phys. Rev. C **71**, 034310 (2005).
[6] M. V. Stoitsov, J. Dobaczewski, W. Nazarewitcz, and P. Ring, Comput. Phys. Commun. **167**, 4363 (2005).
[7] K. Langanke, Nucl. Phys. **A687**, 303 (2001).
[8] J. Stone and P.-G. Reinhard, Prog. Part. Nucl. Phys. (in press).
[9] D. J. Rowe, *Nuclear Collective Motion* (Methuen, London, 1970).
[10] A. Bohr and B. R. Mottelson, *Nuclear Structure* (Benjamin, New York, 1975), Vol. 2.
[11] E. Lipparini and S. Stringari, Nucl. Phys. **A371**, 430 (1981).
[12] T. Suzuki and H. Sagava, Prog. Theor. Phys. **65**, 565 (1981).
[13] T. Kubo, H. Sakamoto, T. Kammuri, and T. Kishimoto, Phys. Rev. C **54**, 2331 (1996).
[14] V. O. Nesterenko, W. Kleinig, V. V. Gudkov, and J. Kvasil, Phys. Rev. C **53**, 1632 (1996).
[15] N. Van Giai, Ch. Stoyanov, and V. V. Voronov, Phys. Rev. C **57**, 1204 (1998).
[16] A. P. Severyukhin, Ch. Stoyanov, V. V. Voronov, and N. Van Giai, Phys. Rev. C **66**, 034304 (2002).
[17] V. O. Nesterenko, W. Kleinig, V. V. Gudkov, N. Lo Iudice, and J. Kvasil, Phys. Rev. A **56**, 607 (1997).
[18] W. Kleinig, V. O. Nesterenko, and P.-G. Reinhard, Ann. Phys. (NY) **297**, 1 (2002).
[19] V. O. Nesterenko, J. Kvasil, and P.-G. Reinhard, Phys. Rev. C **66**, 044307 (2002).
[20] J. Kvasil, V. O. Nesterenko, and P.-G. Reinhard, in *Proceedings of the 7th International Spring Seminar on Nuclear Physics, Miori, Italy, 2001*, edited by A. Covello (World Scientific, Singapore, 2002), p. 437.
[21] V. O. Nesterenko, J. Kvasil, P.-G. Reinhard, W. Kleinig, and P. Fleischer, *Proceedings of the 11th International Symposium on Capture-Gamma-Ray Spectroscopy and Related Topics, Prague, Czech Republic, 2002*, edited by J. Kvasil, P. Cejnar, and M. Krticka (World Scientific, Singapore, 2003), p. 143.
[22] V. O. Nesterenko, J. Kvasil, and P.-G. Reinhard, in *Recent Advances in the Theory of Chemical and Physical Systems*, edited by J.-P. Julien, J. Maruani, D. Mayou, S. Wilson, and G. Delgado-Barrio, serie *Progress in Theoretical Chemistry and Physics*, (Springer, 2006), Vol. 15, p. 127.
[23] V. O. Nesterenko, J. Kvasil, W. Kleinig, P.-G. Reinhard, and D. S. Dolci, arXiv: nucl-th/0512045.
[24] T. H. R. Skyrme, Philos. Mag. **1**, 1043 (1956); D. Vauterin and D. M. Brink, Phys. Rev. C **5**, 626 (1972).

[25] Y. M. Engel, D. M. Brink, K. Goeke, S. J. Krieger, and D. Vauterin, Nucl. Phys. **A249**, 215 (1975).
[26] J. Dobaczewski and J. Dudek, Phys. Rev. C **52**, 1827 (1995).
[27] W. Kohn and L. Sham, Phys. Rev. **140**, A1133 (1965).
[28] O. Gunnarson and B. I. Lundqvist, Phys. Rev. B **13**, 4274 (1976).
[29] W. Kleinig, V. O. Nesterenko, P.-G. Reinhard, and Ll. Serra, Eur. Phys. J. D **4**, 343 (1998).
[30] V. O. Nesterenko, W. Kleinig, F. F. de Souza Cruz, and N. Lo Iudice, Phys. Rev. Lett. **83**, 57 (1999).
[31] V. O. Nesterenko, W. Kleinig, and P.-G. Reinhard, Eur. Phys. J. D **19**, 57 (2002).
[32] V. O. Nesterenko, P.-G. Reinhard, W. Kleinig, and D. S. Dolci, Phys. Rev. A **70**, 023205 (2004).
[33] F. Tondeur, M. Brack, M. Farine, and J. M. Pearson, Nucl. Phys. **A420**, 297 (1984).
[34] J. Bartel, P. Quentin, M. Brack, C. Guet, and H. -B. Håakansson, Nucl. Phys. **A386**, 79 (1982).
[35] E. Chabanat, P. Bonche, P. Haensel, J. Meyer, and R. Schaeffer, Nucl. Phys. **A627**, 710 (1997).
[36] P.-G. Reinhard and H. Flocard, Nucl. Phys. **A584**, 467 (1995).
[37] We now work out the SRPA extension to solve this problem.
[38] P.-G. Reinhard, Ann. Phys. (Leipzig) **1**, 632 (1992).
[39] P.-G. Reinhard, M. Brack, and O. Genzken, Phys. Rev. A **41**, 5568 (1990).
[40] D. J. Thouless, Nucl. Phys. **21**, 225 (1960).
[41] L. A. Malov, V. O. Nesterenko, and V. G. Soloviev, Teor. Mat. Fiz. **32**, 134 (1977).
[42] J. Kvasil, N. Lo Iudice, V. O. Nesterenko, and M. Kopal, Phys. Rev. C **58**, 209 (1998).
[43] T. Sil, S. Shlomo, B. K. Agrawal, and P.-G. Reinhard, Phys. Rev. C **73**, 034316 (2006).
[44] A. S. Goldhaber and G. Scharff-Goldhaber, Phys. Rev. C **17**, 1171 (1978).
[45] JANIS database: l0025.029-0 (Sac1971).
[46] S. S. Dietrich and B. L. Bergman, At. Data Nucl. Data Tables **38**, 199 (1998); IAEA Photonuclear Data.
[47] D. H. Youngblood, Y.-W. Lui, H. L. Clark, B. John, Y. Tokimoto, and X. Chen, Phys. Rev. C **69**, 034315 (2004).
[48] V. O. Nesterenko, V. P. Likhachev, P.-G. Reinhard, V. V. Pashkevich, W. Kleinig, and J. Mesa, Phys. Rev. C **70**, 057304 (2004).
[49] The unperturbed E1 and E2 strengths are provided by transitions via one and two quantum shells, respectively. Hence the stretching effect of the effective mass m_0^*/m is much stronger for E2 than for E1.
[50] P.-G. Reinhard, Nucl. Phys. **A649**, 305c (1999).
[51] M. Brack, C. Guet, and H.-B. Håkansson, Phys. Rep. **123**, 275 (1985).
[52] V. O. Nesterenko, W. Kleinig, J. Kvasil, P. Vesely, and P.-G. Reinhard, to be published in Int. J. Mod. Phys. E.
[53] W. Satula, R. A. Wyss, and M. Rafalski, Phys. Rev. C **74**, 011301(R) (2006).
[54] G. A. Korn and T. M. Korn, *Mathematical Handbook for Scientists and Engineers* (McGraw–Hill, New York, 1968), Chap. 6.5.